American Mineralogist, Volume 75, pages 501–507, 1990

Crystal structure of boggsite, a new high-silica zeolite with the first three-dimensional channel system bounded by both 12- and 10-rings

JOSEPH J. PLUTH, JOSEPH V. SMITH

Department of Geophysical Sciences, Consortium for Theoretical Frameworks, and Materials Research Laboratory, The University of Chicago, Chicago, Illinois 60637, U.S.A.

ABSTRACT

Boggsite, a new zeolite from the Goble area, Oregon, has unit-cell contents $Ca_{7.8}Na_{2.9}Al_{18.3}Si_{77.5}O_{192}\cdot 70H_2O$, an orthorhombic unit cell with $a = 20.236(2)$, $b = 23.798(1)$, $c = 12.798(1)$ Å, and space group *Imma* (74). The four-connected 3-D net linking the tetrahedral vertices has 4-, 5-, 6-, 10- and 12-rings. Three-connected 2-D nets of the gmelinite and ferrierite types occur respectively in the *bc* and *ac* planes. The topology of the 3-D net is obtained by replacing ⅔ of the edges of the gmelinite net by pentasil chains found in the silicalite/ZSM-5/ZSM-11 family of synthetic microporous materials. Each 12-ring channel along **a** has offset 10-ring windows into left and right channels along **b**. Correspondingly, each 10-ring channel is connected to left and right 12-ring channels to yield 3-D access. Each 12-ring is nearly circular with a free diameter between framework oxygens (assumed radius 1.35 Å) of 7.4 by 7.2 Å. Two bifurcated 4-rings reduce the free diameter of each 10-ring (5.2 by 5.1 Å) to approximately that for a near-circular 9-ring. A unique assignment of Ca, Na, and H_2O to the broad irregular peaks in the channels was not achieved. A highly disordered ionic solution that lacks systematic bonding to the silica-rich framework is indicated. The good correlation between mean T-O distance and T-O-T angle indicates Si,Al disorder over all sites.

INTRODUCTION

Zeolites (Gottardi and Galli, 1985) demonstrate the fruitful symbiosis among mineralogists, crystal chemists, and industrial scientists and engineers. Faujasite was discovered in the mid-19th century (Damour, 1842), its crystal structure was determined a century later (Bergerhoff et al., 1958), and its industrial analogues Linde Types X and Y have become important molecular sieves in the chemical and petroleum industries (Breck, 1974; Rabo, 1976). A key feature of the faujasite structure is the 3-D channel system linking large $4^{12}4^66^412^4$ cages via 12-rings with free diameter near 7.5 Å. Synthetic analogues of other natural zeolites are also valuable for industrial applications, including materials related to mordenite, a thermally stable high-silica zeolite whose principal channel is spanned by a 12-ring. Of the synthetic materials not related to natural zeolites, the pentasil family of polytypic materials (silicalite/ZSM-5 and ZSM-11; Flanigen et al., 1978; Kokotailo et al., 1978a, 1978b; Kokotailo and Meier, 1980) and the beta polytypic intergrowth (Higgins et al., 1988; Newsam et al., 1988) are important examples. They are high-silica microporous materials (Jacobs and Martens, 1987) with a 3-D channel system bounded respectively by 10- and 12-rings.

We now illustrate again the fruitful symbiosis in zeolite science. The new mineral boggsite (Howard et al., 1990) has been found to have a 3-D channel system bounded by both 12- and 10-rings. Its tetrahedral framework has a fascinating topology that consists of the union of the 4.6.12 three-connected 2-D net found in gmelinite and the eight-repeat pentasil chain. This new topology extends the classification of the four-connected 3-D nets that was presented in a recent review (Smith, 1988). Synthetic analogues of high-silica boggsite might prove useful as molecular sieves with properties intermediate between those of the above-listed materials.

STRUCTURE DETERMINATION

A small sample of boggsite from the only known locality near Goble, Oregon, was supplied by D. G. Howard. After several attempts to find a suitable single crystal, a euhedral fragment was found that consisted mostly of one crystal. X-ray diffraction photographs showed several additional sets of weak diffractions in nonrational positions. Because of the paucity of the boggsite, it was decided to collect diffraction data for the dominant crystal and ignore any accidental overlap. The fragment is dominated by the {102} and {011} forms described by Howard et al. (1990) and is 0.16 mm along **b**, 0.07 mm along **a** and 0.08 mm along **c**. Irregular overgrowths are probably responsible for the extra diffractions.

The chemical analysis reported by Howard et al. (1990) was used in the interpretation of the crystal structure. Because only one crystal good enough for X-ray crystallographic studies was found, it was kept intact and not modified for electron microprobe analysis. Because the

0003–004X/90/0506–0501$02.00

Table 1. Atomic positions and displacements of boggsite

Atom	Population*	x	y	z	U_{11}**	U_{22}	U_{33}	U_{12}	U_{13}	U_{23}	U_{eq}†
Si(1)	16 × 1.0	0.18881(11)	0.18550(9)	0.6719(2)	0.0189(12)	0.0140(11)	0.0196(12)	−0.0007(9)	0.0007(10)	−0.0024(9)	0.0175(7)
Si(2)	16 × 1.0	0.19006(11)	0.02407(9)	0.3297(2)	0.0214(12)	0.0226(12)	0.0145(11)	0.0001(10)	−0.0028(10)	−0.0002(10)	0.0195(7)
Si(3)	16 × 1.0	0.07689(11)	0.18517(9)	0.8357(2)	0.0164(11)	0.0123(11)	0.0204(12)	0.0003(9)	0.0006(10)	0.0021(9)	0.0164(7)
Si(4)	16 × 1.0	0.07768(11)	0.02210(9)	0.1643(2)	0.0154(11)	0.0226(12)	0.0155(12)	0.0001(9)	0.0007(10)	0.0012(10)	0.0178(7)
Si(5)	16 × 1.0	0.22108(10)	0.08300(9)	0.5378(2)	0.0169(10)	0.0171(11)	0.0176(11)	−0.0012(9)	0.0007(9)	−0.0060(11)	0.0172(6)
Si(6)	16 × 1.0	0.12270(10)	0.08371(9)	0.9656(2)	0.0175(10)	0.0166(12)	0.0176(11)	−0.0017(10)	−0.0002(9)	0.0037(10)	0.0172(6)
O(1)	8 × 1.0	0.1882(4)	¼	0.6291(6)	0.046(5)	0.013(4)	0.032(5)	0	0.002(4)	0	0.030(3)
O(2)	16 × 1.0	0.1194(3)	0.1707(3)	0.7322(5)	0.028(3)	0.034(4)	0.041(4)	−0.004(3)	0.009(3)	−0.009(3)	0.034(2)
O(3)	16 × 1.0	0.1950(3)	0.1456(2)	0.5679(4)	0.053(4)	0.025(3)	0.026(3)	0.006(3)	0.000(3)	−0.008(3)	0.035(2)
O(4)	16 × 1.0	0.1900(3)	0.0702(2)	0.4236(4)	0.051(4)	0.037(4)	0.020(3)	0.007(3)	−0.008(3)	−0.011(3)	0.036(2)
O(5)	16 × 1.0	0.1194(3)	0.0319(3)	0.2722(5)	0.024(3)	0.059(5)	0.026(4)	−0.001(3)	−0.008(3)	−0.004(3)	0.036(2)
O(6)	16 × 1.0	0.0893(4)	¼	0.8731(6)	0.037(5)	0.017(4)	0.031(5)	0	−0.014(4)	0	0.028(3)
O(7)	8 × 1.0	0	0.1738(3)	0.8043(7)	0.012(4)	0.033(5)	0.049(6)	0	0	−0.013(4)	0.031(3)
O(8)	8 × 1.0	0	0.0263(4)	0.1968(7)	0.018(4)	0.070(7)	0.033(5)	0	0	−0.004(5)	0.040(3)
O(9)	16 × 1.0	0.1944(4)	0.0379(3)	0.6204(5)	0.104(6)	0.028(4)	0.030(4)	−0.013(4)	0.016(4)	0.008(3)	0.054(3)
O(10)	16 × 1.0	0.0978(3)	0.1464(2)	0.9327(5)	0.069(4)	0.015(3)	0.034(4)	0.006(3)	−0.006(3)	0.008(3)	0.039(2)
O(11)	16 × 1.0	0.0959(3)	0.0725(3)	0.0813(5)	0.067(4)	0.037(4)	0.027(4)	−0.007(3)	0.016(3)	0.008(3)	0.044(2)
O(12)	16 × 1.0	0.2007(3)	0.0800(3)	0.9682(6)	0.014(3)	0.103(6)	0.096(6)	−0.002(4)	0.004(4)	0.044(5)	0.071(3)
O(13)	16 × 1.0	0.0949(3)	0.0395(3)	0.8847(5)	0.079(5)	0.025(4)	0.035(4)	−0.011(4)	−0.014(4)	−0.004(3)	0.046(2)
O(14)	8 × 1.0	¼	0.1755(3)	¾	0.039(5)	0.033(5)	0.050(6)	0	−0.022(5)	0	0.040(3)
O(15)	8 × 1.0	¼	−0.0375(4)	¾	0.027(5)	0.069(7)	0.031(5)	0	−0.010(4)	0	0.043(3)
W(1)‡	8 × 1.85(7)	0	0.1735(11)	0.136(2)	—	—	—	—	—	—	0.70(4)
W(2)	16 × 1.35(5)	0.1936(10)	0.1701(11)	0.203(2)	—	—	—	—	—	—	0.48(2)
W(3)	8 × 0.92(6)	0.193(2)	¼	0.057(2)	—	—	—	—	—	—	0.25(2)
W(4)	16 × 1.16(6)	0.1074(14)	0.1754(13)	0.372(2)	—	—	—	—	—	—	0.43(3)
W(5)	8 × 3.2(2)	0	0.175(2)	0.570(3)	—	—	—	—	—	—	1.44(9)
W(6)	8 × 0.91(4)	0	0.0284(15)	0.429(2)	—	—	—	—	—	—	0.33(3)
W(7)	16 × 0.63(4)	0.0562(14)	0.1147(14)	0.410(3)	—	—	—	—	—	—	0.25(2)
W(8)	16 × 0.77(4)	0.0431(9)	0.0812(11)	0.626(2)							0.27(2)
W(9)	8 × 0.50(5)	0.149(2)	¼	0.237(3)							0.18(3)
W(10)	8 × 0.61(5)	0.106(2)	¼	0.086(3)							0.19(3)
W(11)	8 × 1.32(7)	0.206(2)	¼	0.401(3)							0.44(3)

* Population given as site multiplicity × fractional occupancy.

** U_{ij} are defined as $\exp(-2\pi^2 \sum_{i=1}^{3} \sum_{j=1}^{3} U_{ij} a_i^* a_j^* h_i h_j)$.

† U_{eq} is defined as $\frac{1}{3} \sum_{i=1}^{3} \sum_{j=1}^{3} U_{ij} a_i^* a_j^* (\mathbf{a}_i \cdot \mathbf{a}_j)$ or isotropic displacement factor.

‡ O scattering factors were used for W.

positions of the Na, Ca, and H_2O could not be located, any uncertainty in their relative proportions is unimportant here.

The crystal was mounted on an automated Picker-Krisel four-circle diffractometer with b offset 1° from the ϕ axis. Refinement using 20 diffractions ($50 < 2\theta < 82°$; $\lambda = 1.5418$ Å), each the average of automatic centering of eight equivalent settings, gave orthogonal cell parameters $a = 20.236(2)$, $b = 23.798(1)$, $c = 12.798(1)$ Å. No adjustment in cell repeats was made for asymmetric absorption. A total of 11 231 intensities was collected with the θ-2θ technique, scan speed 2°/min, and scan width 1.6–2.2° for range 3.0–128° 2θ. Merging, as consistent with the orthorhombic system, yielded 2718 intensities ($R_{int} = 0.036$), all of which were used in refinements: data-collection range $h \pm 22$, $k + 26$, $l \pm 14$; mean intensity variation of three standard reflections 3%. No absorption correction was applied because the crystal was small and had a complicated, fragmented shape ($\mu = 72$ cm^{-1}). The systematic absences indicate a body-centered lattice and the coupled a and b glide planes normal to c. Of the three possible space groups, $Im2a(46)$, $I2mb(46)$, and $Imma(74)$, the centrosymmetric one proved adequate for the structure determination. Removal of the center of symmetry did not improve the final R-factors significantly. The initial model derived from MULTAN 80 (Main, 1980) was refined by Fourier methods. Least-squares refinement led to accurate coordinates for the six T and fifteen O atoms. A difference-Fourier map showed broad irregular peaks in the channels. In spite of detailed attempts to locate Na, Ca, and H_2O atoms, a truly reliable answer proved elusive. Such an unsatisfactory outcome is typical for the contents of wide channels and the large cages of zeolites (e.g., faujasite; Baur, 1964). Although positions of extraframework peaks are listed in Table 1, no chemical interpretation can be offered, and the discussion is confined to the framework.

In the final model, 218 variables were refined including scale factor, positions for 21 framework atoms and 11 nonframework peaks, anisotropic displacement factors for framework atoms, and isotropic ones for nonframework peaks. Note that the population factors and anisotropic displacement factors of the nonframework peaks are very uncertain and are listed merely for technical reasons. Neutral scattering factors from International Tables for X-ray Crystallography (Ibers and Hamilton, 1974) were

Table 2. Boggsite framework interatomic distances (Å) and angles (°)

Si(1)-O(1)	1.630(4)	1.642(4)*	O(1)-Si(1)-O(2)	110.7(4)
Si(1)-O(2)	1.641(6)	1.655(6)	O(1)-Si(1)-O(3)	105.8(3)
Si(1)-O(3)	1.640(6)	1.655(6)	O(1)-Si(1)-O(14)	110.7(4)
Si(1)-O(14)	1.609(3)	1.630(4)	O(2)-Si(1)-O(3)	108.9(3)
Mean	1.630	1.646	O(2)-Si(1)-O(14)	109.6(3)
			O(3)-Si(1)-O(14)	111.1(3)
Si(2)-O(4)	1.626(6)	1.642(6)*	O(4)-Si(2)-O(5)	105.0(3)
Si(2)-O(5)	1.619(6)	1.634(6)	O(4)-Si(2)-O(9)	109.0(3)
Si(2)-O(9)	1.610(7)	1.642(7)	O(4)-Si(2)-O(15)	109.5(4)
Si(2)-O(15)	1.617(3)	1.638(4)	O(5)-Si(2)-O(9)	109.5(4)
Mean	1.618	1.639	O(5)-Si(2)-O(15)	110.6(2)
			O(9)-Si(2)-O(15)	113.0(4)
Si(3)-O(2)	1.615(6)	1.630(7)*	O(2)-Si(3)-O(6)	111.0(4)
Si(3)-O(6)	1.635(3)	1.645(4)	O(2)-Si(3)-O(7)	105.7(4)
Si(3)-O(7)	1.630(3)	1.644(4)	O(2)-Si(3)-O(10)	111.8(3)
Si(3)-O(10)	1.604(6)	1.624(7)	O(6)-Si(3)-O(7)	112.1(4)
Mean	1.621	1.636	O(6)-Si(3)-O(10)	106.0(4)
			O(7)-Si(3)-O(10)	110.3(4)
Si(4)-O(5)	1.635(6)	1.651(6)*	O(5)-Si(4)-O(8)	105.9(4)
Si(4)-O(8)	1.629(3)	1.648(4)	O(5)-Si(4)-O(11)	109.0(3)
Si(4)-O(11)	1.644(7)	1.667(7)	O(5)-Si(4)-O(13)	110.0(3)
Si(4)-O(13)	1.632(7)	1.659(7)	O(8)-Si(4)-O(11)	109.7(4)
Mean	1.635	1.656	O(8)-Si(4)-O(13)	111.1(4)
			O(11)-Si(4)-O(13)	111.0(3)
Si(5)-O(3)	1.628(6)	1.642(6)*	O(3)-Si(5)-O(4)	105.1(3)
Si(5)-O(4)	1.621(6)	1.638(6)	O(3)-Si(5)-O(9)	110.4(3)
Si(5)-O(9)	1.600(7)	1.636(7)	O(3)-Si(5)-O(12)	112.1(4)
Si(5)-O(12)	1.587(6)	1.639(6)	O(4)-Si(5)-O(9)	109.8(3)
Mean	1.609	1.639	O(4)-Si(5)-O(12)	109.5(4)
			O(9)-Si(5)-O(12)	109.9(4)
Si(6)-O(10)	1.630(6)	1.651(6)*	O(10)-Si(6)-O(11)	106.7(3)
Si(6)-O(11)	1.599(6)	1.624(7)	O(10)-Si(6)-O(12)	111.4(4)
Si(6)-O(12)	1.580(6)	1.633(6)	O(10)-Si(6)-O(13)	109.3(3)
Si(6)-O(13)	1.580(7)	1.607(7)	O(11)-Si(6)-O(12)	108.0(4)
Mean	1.597	1.629	O(11)-Si(6)-O(13)	112.0(3)
			O(12)-Si(6)-O(13)	109.4(4)
Si(1)-O(1)-Si(1)	140.7(6)		Si(1)-O(2)-Si(3)	142.7(4)
Si(1)-O(3)-Si(5)	138.3(4)		Si(2)-O(4)-Si(5)	142.5(4)
Si(2)-O(5)-Si(4)	145.5(4)		Si(3)-O(6)-Si(3)	141.3(6)
Si(3)-O(7)-Si(3)	145.4(6)		Si(4)-O(8)-Si(4)	149.6(6)
Si(2)-O(9)-Si(5)	153.5(5)		Si(3)-O(10)-Si(6)	143.9(4)
Si(4)-O(11)-Si(6)	142.8(4)		Si(5)-O(12)-Si(6)	172.9(6)
Si(4)-O(13)-Si(6)	157.8(5)		Si(1)-O(14)-Si(1)	163.0(6)
Si(2)-O(15)-Si(2)	157.2(7)			
Selected distances (Å) across 12-ring channel				
O(15)-O(15)	10.12(2)			
O(5)-O(5)	10.38(2)			
O(1)-O(6)	9.88(1)			
O(3)-O(10)	9.72(1)			
O(4)-O(11)	9.75(1)			
Selected distances (Å) across 10-ring channel				
O(9)-O(9)	7.88(2)			
O(4)-O(4)	7.69(1)			
O(4)-O(9)	8.21(1)			
O(5)-O(5)	7.72(1)			
O(8)-O(8)	7.86(2)			

* Adjusted for riding of O on Si.

used; a common factor for $Si_{0.81}Al_{0.19}$ was used for all six T atoms. The final least-squares refinement minimized all Fs with σ_F computed from σ_I, the square root of [total counts + (2% of total counts)²]. The resulting criteria are $w = \sigma_F^{-2}$, $R = 0.092$, $wR = 0.094$, $S = 5.7$, largest shift/e.s.d. = −0.14 for x of W(9); maximum and minimum heights on final difference-Fourier map +1.7 and −0.8 eÅ^{-3}. The computer programs used were a local data reduction system, SHELX76 (Sheldrick, 1976), ORFFE (Busing et al., 1964), and ORTEP (Johnson, 1976). Final atomic coordinates and displacement parameters are given in Table 1, interatomic distances (with and without riding motion) and angles in Table 2 and a calculated powder diffraction pattern in Table 3 (POWD computer program; Smith and Smith, 1986). The observed and calculated structure factors are given in Table 4.[1]

Table 3. Calculated powder pattern for boggsite

d	I/I_0	*hkl*	*d*	I/I_0	*hkl*
11.899	33	020	3.083	5	343
11.271	100	011	3.051	3	204
10.816	27	101	2.975	9	080
10.118	24	200	2.936	6	503
8.004	6	121	2.936	3	134
7.708	3	220	2.875	6	163
6.742	15	031	2.870	3	314
5.967	10	301	2.818	5	044
5.910	3	112	2.778	5	552
5.636	7	022	2.668	4	363
5.408	2	202	2.633	15	543
5.059	5	400	2.590	11	091
4.924	5	222	2.548	2	741
4.556	6	312	2.530	2	800
4.461	34	051	2.500	2	732
4.357	31	042	2.471	2	354
4.213	4	341	2.436	5	035
4.174	2	103	2.393	2	703
4.007	11	332	2.393	2	534
4.002	2	242	2.368	2	235
3.966	3	060	2.360	4	563
3.878	2	213	2.298	2	761
3.859	86	501	2.247	3	093
3.757	13	033	2.133	3	0,11,1
3.753	2	152	2.049	3	365
3.693	6	260	2.024	7	10,0,0
3.671	13	521	1.9843	7	804
3.605	31	303	1.9832	2	0,12,0
3.522	7	233	1.9788	2	853
3.417	5	143	1.9511	7	394
3.386	31	512	1.8702	2	356
3.373	2	600	1.8204	4	594
3.371	63	062	1.7940	2	815
3.323	7	352	1.6429	4	0,14,2
3.303	8	361	1.6306	2	806
3.200	3	004	1.6044	2	547
3.198	9	262	1.6007	2	5,10,5
3.177	4	052	1.5884	2	0,10,6
3.141	2	532	1.5745	2	0,15,1

Discussion

Topology

Stereoplots (Figs. 1 and 2) show the tetrahedral vertices and T-T edges of the four-connected net. Four structural features are important: (1) single 8-repeat chains of pentasil type (labeled **p**; Smith, 1988), of which two are emphasized in Figure 1; (2) double pentasil chains (**pp**), each of which lies between two **p** chains; (3) 4.6.12 three-connected 2-D nets (Fig. 3) of gmelinite type (*gme*) that are strongly distorted from ideal geometry, as shown by heavy lines at the bottom of Figure 1; (4) three-connected 2-D nets of ferrierite type (*fer,* Figure 4) consisting of 5-, 6- and 10-rings that are considerably crinkled (front surface

[1] A copy of Table 4 may be ordered as Document AM-90-431 from the Business Office, Mineralogical Society of America, 1625 I Street, N.W., Suite 414, Washington, D.C. 20006, U.S.A. Please remit $5.00 in advance for the microfiche.

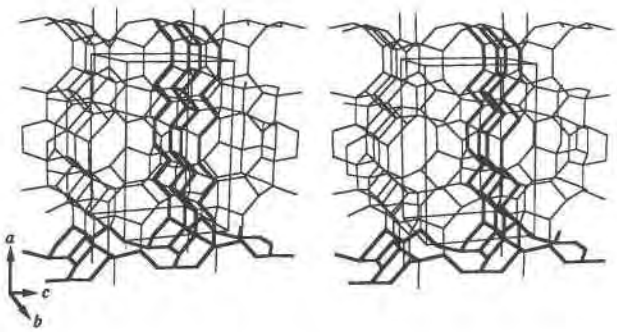

Fig. 1. Four-connected 3-D net linking tetrahedral vertices of boggsite. One double-pentasil and two single pentasil chains parallel to *a* are highlighted. A very distorted 4.6.12 three-connected 2-D net (*gme*) in the *bc* plane is also highlighted. On the front face of the stereoplot is a distorted *fer* net containing 5-, 6- and 10-rings. Only one-half the *b* repeat is shown, centered about $b = 0.25$.

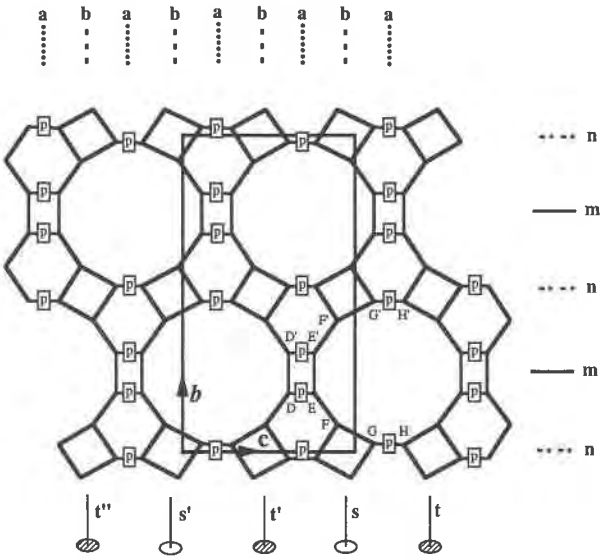

Fig. 3. Replacement of ⅔ of the edges of the 4.6.12 net by projections of pentasil chains. The hexagonal symmetry of the ideal net is lowered to rectangular *cmm* plane-group symmetry for the *bc* section of boggsite.

of Fig. 1). The simplest topological description of the BOG type of four-connected 3-D net is the replacement of ⅔ of the edges of the *gme* 2D net by **p** chains (Fig. 3). This results in double-pentasil chains generated from opposite edges of ⅓ of the 4-rings and single-pentasil chains from ⅓ of the edges of the 6-rings. Each pentasil chain (Fig. 1) has a parallel edge alternating on the left or right with a zig-zag-zig or zag-zig-zag intervening sequence of three edges.

Channel system

The staggered arrangement of 12- and 10-rings in the four-connected 3-D net generates a 3-D system of intersecting channels. To understand the connectivity, it is important to consider the symmetry control of the space group *Imma*. The positions of the planes of symmetry are shown in Figures 3 and 4. Note that the interaction with the body centering generates the *n* glide planes normal to *a* and *b* that lie midway between mirror planes in those directions, and the *b* glide plane lying halfway between *a* glide planes normal to *c*.

Comparison of the stereoplot of Figure 2 with the projection of Figure 3 shows that a 10-ring lies in the surface of a 12-ring channel at positions labeled DEFGH. The two vertices labeled D are joined by a vertical edge of a pentasil chain, as are those labeled H. The pairs of edges DE and GH also belong to pentasil chains. Vertices D′-H′ generate another 10-ring at the same height along *a* that is related to DH by the mirror plane normal to *b*. These two 10-rings are repeated along the **b** axis to yield a straight 10-ring channel, labeled s in Figure 3. The *c*-repeat produces the channel labeled s′. A second set of 10-ring channels is generated by the *a* glide plane normal to *c* in Figure 3. This set (t, t′, t″, etc.) is offset by the body-centering vector from the first set. The offsets of the 10-ring channels with respect to the 12-ring channel are responsible for the 3-D connectivity in boggsite. Such a 3-D connectivity is highly prized for potential molecular sieves, since blockage of the channel system is much less likely than for 2-D or 1-D connectivity.

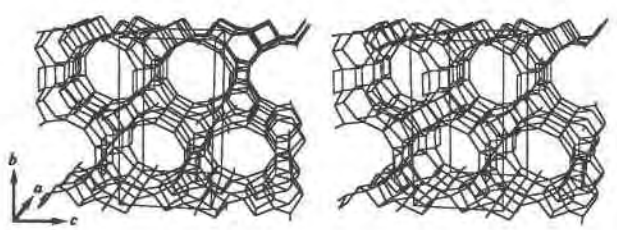

Fig. 2. Four-connected 3-D net linking tetrahedral vertices of boggsite. The 12-ring channels are generated by replacement of ⅔ of the edges of the 4.6.12 net by pentasil chains.

Comparison of the stereoplot in Figure 1 with the projection in Figure 4 shows that the 12-rings occur in projection at PQRSTU and PQRS′T′U′, together with symmetry-related positions. Note the two types of 12-rings, only one of which is highlighted in Figure 1: STU are not related by symmetry to S′T′U′. Just as for the 10-rings in Figure 3, the 12-rings of Figure 4 lie at different levels as required by the body-centering translation.

Figures 5 and 6 show the open cross-sections of the 12- and 10-ring channels on the standard assumption that each framework O atom acts like a hard sphere of radius 1.35 Å (Breck, 1974, p. 633 et seq.). Because the 12-rings are nonplanar and not perpendicular to the channel axis, the cross section is reduced slightly from the maximum value (~7.5 Å) for a circular 12-ring to a near-circular aperture approximately 7.4 × 7.2 Å in dimensions (defined by O(5)-O(15) and O(1)-O(6)). The 10-ring channel has two pairs of edges that each belong to a 4-ring in the

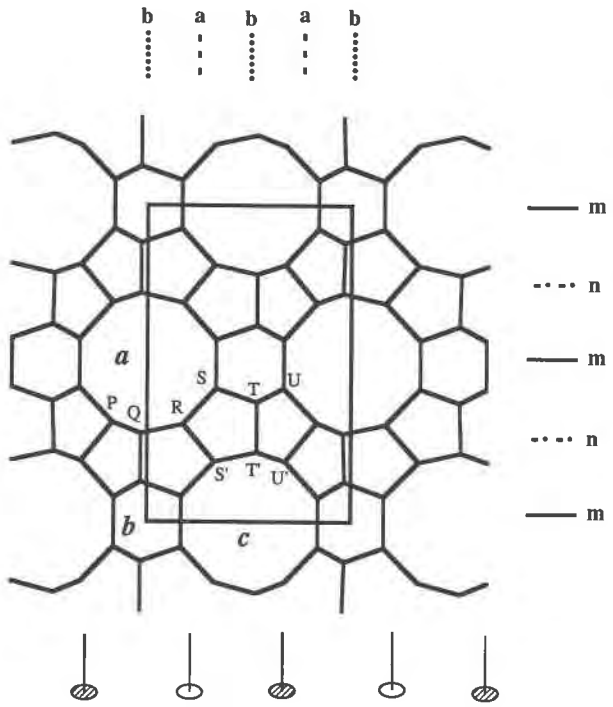

Fig. 4. Projection of the distorted *fer* net of boggsite onto the *ac* plane.

channel wall. Consequently these four edges are shortened about 30% in projection. Hence the 10-ring channel has a cross-section 5.2 × 5.1 Å (defined by O(8)-O(8) and the average of O(9)-O(9) and O(4)-O(4)), slightly smaller than that for an ideal circular 9-ring.

Polyhedral subunits of the four-connected net

Polyhedral subunits of 4-connected 3-D nets are of interest because they can be connected in different ways to generate new 3-D nets, and because they might be useful in discussions about crystallization. Figure 7 shows some useful polyhedral subunits. The ***bru*** unit, $4^2 5^4$ (i.e., two symmetry-related 4-rings and four 5-rings), also occurs in the 3-D-nets of brewsterite, heulandite, stilbite, and scapolite (Smith, 1989); stereoplots of some but not all nets are given in Meier and Olson (1987). The ***bru*** unit can be described as a 1,3-stellated cube because single edges in the 1 and 3 positions of a cube are replaced by two edges sharing a two-connected vertex. The ***bog*** unit, $4^2 6^4$-b, can be described as a 1,3-handle cube in which the 1 and 3 edges are replaced by three edges sharing two two-connected vertices. The ***lov*** unit, $4^2 6^2$, is a 1,3-open cube that is obtained by removing the 1 and 3 edges. It occurs in eight other frameworks ($AlPO_4$-11, $AlPO_4$-5, $AlPO_4$-D, laumontite, lovdarite, feldspar, banalsite, and $AlPO_4$-54/VPI-5), and is present in both the ***bru*** and ***bog*** units. The ***pes*** unit, $5^2 6^2$, is the penta-edge-stellated tetrahedron that also occurs in eight other frameworks (bikitaite, mordenite, ZSM-23, ZSM-12, Theta-1, $CsAlSi_5O_{12}$, ZSM-57, and EU-1). Finally, two ***pes*** units can share a 6-ring to give the ***eun*** unit that occurs in the $CsAlSi_5O_{12}$ and EU-1 nets as well as in the boggsite net.

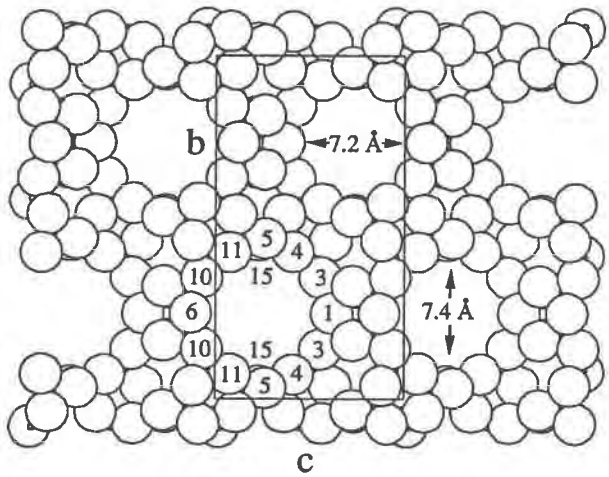

Fig. 5. Sphere packing of O atoms in a *gml* layer of boggsite. Labels are given for O atoms of one 12-ring and for two O(15). Some T positions are shown by small circles.

Figure 8 shows how the polyhedral subunits are linked together. At the center (the unit-cell origin) is a ***lov*** unit. Above and below it are ***bru*** units, each sharing one of the 4-rings of the ***lov*** unit. Flanking each ***bru*** unit to the east and west are two ***eun*** units, each of which shares a 5-ring with the ***bru*** unit. This cluster of one ***lov***, two ***bru*** and four ***eun*** is completed by addition of two vertical edges that convert the ***lov*** unit into the ***bog*** unit. Each of these edges links a vertex from each of two ***eun*** units that are

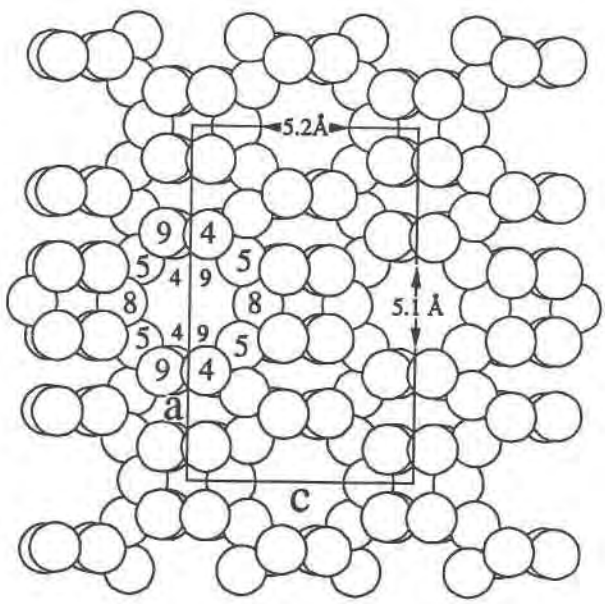

Fig. 6. Sphere packing of oxygen atoms in an *fer* layer of boggsite. Labels are given for one 10-ring. Two bifurcations occur for the O(4) and O(9) atoms.

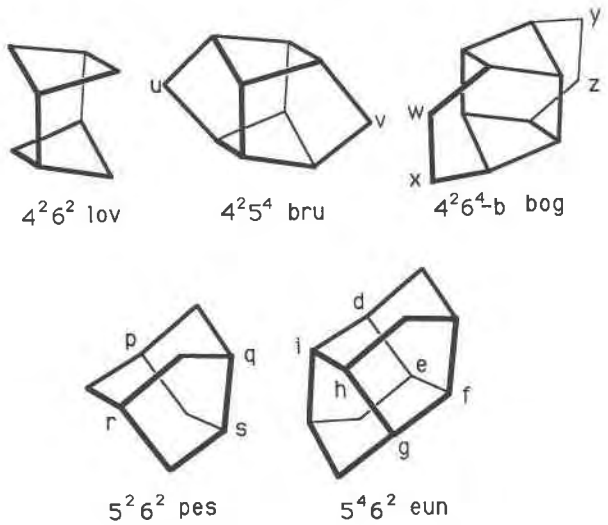

Fig. 7. Polyhedral subunits in boggsite.

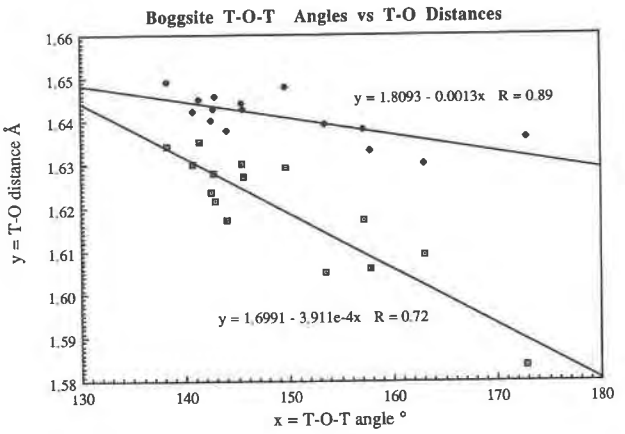

Fig. 9. T-O distance versus T-O-T angle. Open square, uncorrected for riding motion; filled diamond, adjusted for O riding on T atom.

related by a horizontal mirror operation. The augmented cluster of one ***bog***, two ***bru***, and four ***eun*** has four strings of seven edges, each of which becomes part of a pentasil chain. Viewed from above, the augmented cluster projects as a 4-ring flanked on opposite sides by two 6-rings. This is part of the 4.6.12 three-connected 2-D net of *gml* type.

Tetrahedral geometry and Al,Si disorder

At first sight the range of mean T-O distances for the six independent tetrahedra (1.597 to 1.635 Å) might suggest that the Al is concentrated in the larger tetrahedra. However, there is an excellent correlation between the T_i-O_j-T_k angle and the mean T_i-O and T_k-O distances for the 15 independent O_j atoms (Figure 9). The correlation is better for distances adjusted for riding motion than for distances obtained from centroids in least-squares refinement. Because the scatter about the best-fit line for riding-adjusted distances is within 2σ experimental error, it is concluded that there is no evidence for preferential occupancy of Si and Al among the six T sites.

From the general viewpoint of the interpretation of the bonding in aluminosilicates, Figure 9 indicates that the purely technical role of riding motion must be considered. The slope of the best-fit regression line is reduced about threefold when the distances are adjusted for riding motion. This point is not pursued any further in this paper, and readers are referred to Geisinger et al. (1987) and Smyth et al. (1987) for relevant experimental data for coesite, which has a range of T-O-T angles (137–180°) similar to that of boggsite (138–173°). Incidentally, the largest T-O-T angle in boggsite (173°) is similar to that for various zeolites listed by Alberti (1986). The increase in the atomic displacement factor with the T-O-T angle for boggsite (data in Tables 1 and 3; graphic implication from riding-motion adjustment in Figure 9) is relevant to Alberti's argument that a T-O-T angle of 180° does not occur in zeolites. There is a large disc-shaped displacement ellipsoid for O(12) whose T(5)-O(12)-T(6) angle is 173°. An angle of 180° does occur in coesite, and it may not be necessary to assume that there is static disorder for all or some O atoms in zeolites that have a T-O-T angle of 180°.

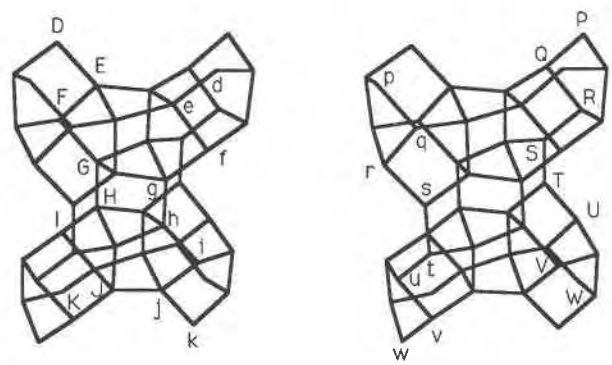

Fig. 8. Stereoplot of the cluster of one ***bog***, two ***bru***, and four ***eun*** units. Vertices D-K and d-k are part of single pentasil chains, and vertices P-W and p-w are part of pentasil chains that are doubled up in the boggsite net.

Extraframework species

All the electron density in the channels is represented by weak, broad, and ill-defined peaks. None of the sites obtained by purely mathematical refinement is within 2.8 Å of a framework O. The obvious conclusion is that the cations and water molecules are interacting only weakly with the aluminosilicate framework.

Future research

The present structure analysis opens up many possible research problems.

1. Synthesis of a large sample of boggsite-type material

is highly desirable to allow thorough investigation of its potential use as a molecular sieve and catalyst. The presence of 5-rings almost certainly rules out an $AlPO_4$-type composition because of the ubiquitous alternation of Al and P in known microporous aluminophosphates. Silica-rich systems offer the most promise. Computer modeling might indicate that a particular organic material might act as a template. That boggsite occurs in only one locality so far among the huge expanse of flood basalts in the northwestern United States indicates that somewhat special conditions were involved that precluded the crystallization of the more abundant zeolites listed in Gottardi and Galli (1985). If those conditions could be identified, some clues might be obtained that would guide a search for conditions of crystallization for boggsite. Certainly the presence of Ca and Na in boggsite offers little guide to synthesis conditions, especially as those cations are not tightly bonded to the tetrahedral framework.

2. From the strictly crystallographic viewpoint, it would be valuable to make structure determinations for dehydrated boggsite and for ion-exchanged varieties. High-intensity X-ray sources, including synchrotrons, allow the use of even smaller crystals than the one used here.

3. The topological features of boggsite act as a trigger for further exploration of new types of four-connected 3-D nets. A systematic study of the union of pentasil chains and three-connected 2-D nets is yielding many new 3-D nets. The polyhedral subunits found in boggsite can also be linked together in different ways. The simplest way to invent a new net from the boggsite net is to convert each double-pentasil chain into a single pentasil chain. The resulting net retains a 3-D channel system, but each 12-ring is reduced to a 10-ring. The space group *Imma* (74) is retained, as are the *a* and *c* repeats; however, *b* is reduced to ~17.6 Å. In the Catalog of Frameworks of the Consortium for Theoretical Frameworks, the boggsite net is assigned number 636, and the new net becomes 650.

To conclude, these opportunities for further research and development reaffirm the importance of geology and mineralogy for chemical research and industrial applications. They would have delighted Glauco Gottardi, to whom this paper is dedicated.

Acknowledgments

We thank Donald G. Howard and Ruby Tschernich for the opportunity to do a structure analysis on their crystals. Their persistent enthusiasm in the field and patient search in the optical laboratory were the key to success. Nancy Weber prepared an elegant manuscript. Financial assistance from NSF CHE 8618041 (JVS), NSF DMR 8519460 (JJP), and the Consortium for Theoretical Frameworks (Exxon Education Foundation, Union Carbide Corporation, and UOP) is greatly appreciated.

References cited

Alberti, A. (1986) The absence of T-O-T angles of 180° in zeolites. In Y. Murakami, A. Iijima, and J.W. Ward, Eds., New developments in zeolite science, p. 437–441. Technology, Kodansha, Tokyo.

Baur, W.H. (1964) On the cation and water positions in faujasite. American Mineralogist, 49, 697–704.

Bergerhoff, G., Baur, W.H., and Nowacki, W. (1958) Über die Kristallstrukturen des Faujasits, Neues Jahrbuch für Mineralogie Monatshefte, 193–200.

Breck, D.W. (1974) Zeolite molecular sieves. Wiley, New York.

Busing, W.R., Martin, K.O., and Levy, H.A. (1964) ORFFE: A Fortran crystallographic function and error program, ORNL-TM-306, Oak Ridge National Laboratory, Oak Ridge, Tennessee.

Damour, A.A. (1842) Description de la faujasite, nouvelle espéce minérale. Annales des Mines, ser. 4, 1, 395–399.

Flanigen, E.M., Bennett, J.M., Grose, R.W., Cohen, J.P., Patton, R.L., Kirchner, R.M., and Smith, J.V. (1978) Silicalite, a new hydrophobic crystalline silica molecular sieve. Nature, 271, 512–516.

Geisinger, K.L., Spackman, M.A., and Gibbs, G.V. (1987) Exploration of structure, electron density distribution, and bonding in coesite with Fourier and pseudoatom refinement methods using single-crystal X-ray diffraction data. Journal of Physical Chemistry, 91, 3237–3244.

Gottardi, G., and Galli, E. (1985) Natural zeolites. Springer-Verlag, Berlin.

Higgins, J.B., LaPierre, R.B., Schlenker, J.L., Rohrman, A.C., Wood, J.D., Kerr, G.T., and Rohrbaugh, W.J. (1988) The framework topology of zeolite beta. Zeolites, 8, 446–452.

Howard, D.G., Tschernich, R.W., Smith, J.V., and Klein, G.L. (1990) Boggsite, a new high silica zeolite from Goble, Columbia County, Oregon. American Mineralogist, in press.

Ibers, J.A., and Hamilton, W.C., Eds. (1974) International tables for X-ray crystallography, vol. IV, 99–101. Kynoch Press, Birmingham, England.

Jacobs, P.A., and Martens, J.A. (1987) Synthesis of high-silica aluminosilicate zeolites. Elsevier, Amsterdam.

Johnson, C.K. (1976) ORTEP-II: A Fortran thermal ellipsoid plot program for crystal structure illustrations, ORNL-3794, Oak Ridge National Laboratory, Oak Ridge, Tennessee.

Kokotailo, G.T., Lawton, S.L., Olson, D.H., and Meier, W.M. (1978a) Structure of synthetic zeolite ZSM-5. Nature, 272, 437–438.

Kokotailo, G.T., Chu, P., Lawton, S.L., and Meier, W.M. (1978b) Synthesis and structure of synthetic zeolite ZSM-11. Nature, 275, 119–120.

Kokotailo, G.T., and Meier, W.M. (1980) Pentasil family of high silica crystalline materials. Chemical Society Special Publication, 33, 133–139.

Main, P. (1980) MULTAN80: A system of computer programs for the automatic solution of crystal structures from X-ray diffraction data. University of York, York, England.

Meier, W.M., and Olson, D.H. (1987) Atlas of zeolite structure types, 2nd revised edition, Butterworth's, London.

Newsam, J.M., Treacy, M.M.J., Koetsier, W.T., and De Gruyter, C.B. (1988) Structural characterization of zeolite beta. Proceedings of the Royal Society of London, A 420, 375–405.

Rabo, J.A. (1976) Zeolite chemistry and catalysis. American Chemical Society Monograph 171.

Sheldrick, G.M. (1976) SHELX-76: A program for crystal structure determination. Cambridge University, Cambridge, England.

Smith, D.K., and Smith, K.L. (1986) POWD: A Fortran-77 program for calculating X-ray powder diffraction patterns. Pennsylvania State University, University Park, Pennsylvania.

Smith, J.V. (1988) Topochemistry of zeolites and related materials. 1. Topology and geometry. Chemical Reviews, 88, 149–182.

——— (1989) Towards a comprehensive mathematical theory for the topology and geometry of microporous materials. In P.A. Jacobs and R.A. van Santen, Eds., Zeolites: Facts, figures, future, p. 29–47. Elsevier, Amsterdam.

Smyth, J.R., Smith, J.V., Artioli, G., and Kvick, Å. (1987) Crystal structure of coesite, a high-pressure form of SiO_2, at 15 and 298 K from single-crystal neutron and X-ray diffraction data: Test of bonding models. Journal of Physical Chemistry, 91, 988–992.

Manuscript received September 18, 1989
Manuscript accepted February 26, 1990